Experimental Investigation of Transonic Flow Past a Blunt Cone-Cylinder

M. A. Ramaswamy* and G. Rajendra†
National Aeronautical Laboratory, Bangalore, India

The flow past a blunt cone-cylinder at transonic speeds and at moderate angles of incidence has been studied experimentally by recording 1) the longitudinal and circumferential pressure distribution, 2) the surface oil flow patterns using a suspension of titanium dioxide in oleic acid. The results indicate some interesting three-dimensional flow separation phenomenon at transonic speeds.

Nomenclature

C_p = pressure coefficient
C_p^* = pressure coefficient at local sonic condition
D = body diameter
M_∞ = freestream Mach number
Re_D = Reynolds number based on cylinder diameter
X/D = nondimensionalized distance from nose
α = angle of incidence

Introduction

A BLUNT cone-cylinder is a typical configuration for rockets, missiles, and launch vehicles. From both aerodynamic and structural points of view, the study of flow phenomenon on such vehicles is of importance at transonic speeds as it entails the presence of shock waves and associated boundary-layer interaction effects.[1-3] Although theoretical methods have been developed recently for transonic speeds, they are generally not capable of tackling such shock-wave/boundary-layer interactions. An experimental investigation was therefore undertaken on a blunt cone-cylinder with semicone angle of 20 deg in the Mach number range 0.5-0.95 and at angles of incidence 0, 5, and 10 deg. The model blockage at zero incidence was kept at a low value of 0.34% to minimize the interference effects.

Experimental Details

Tunnel

The tests on the model were conducted in the 4-ft Trisonic Wind Tunnel[4] of the National Aeronautical Laboratory. This blowdown tunnel has a Mach number capability of 0.2-4.0. The top and bottom walls of the transonic test section have holes with 6% open area ratio inclined at 30 deg to the flow direction, and the side walls have holes normal to the surface with 20% open area ratio.

Model

The model is a blunt cone-cylinder 80 mm in diameter with a 20 deg semivertex angle and a spherical nose of radius 10 mm. It has a total of 50 pressure orifices of 0.5 mm diameter provided at various longitudinal intervals on two diametrically opposite meridians.

Test Conditions

The tests were conducted at a stagnation pressure of 25 psia and a stagnation temperature of approximately 300 K. The Reynolds number of the tests based on diameter of the model varied from 1.4×10^6 at $M_\infty=0.52$ to 2.0×10^6 at $M_\infty=0.94$.

Pressure Measurement

The pressure measurements were obtained using a 48-port pressure scanner. On-line recording of the pressure from one of the channels was done to ensure pressure stabilization before trapping the pressures in storage volumes by means of cutoff valves. Using the pressure scanner, the trapped pressures were sequentially measured by a ±25 psid differential Statham pressure transducer.

Oil Flow Visualization Technique

A mixture of titanium dioxide, oleic acid, and high-vacuum oil in suitable proportions was sprayed on the model before a run. The streamline patterns obtained were photographed just after the run. The model was painted black to obtain good contrast.

Results and Discussions

Longitudinal Pressure Distribution at Zero Incidence

Longitudinal pressure distributions for zero incidence at $M_\infty=0.52$, 0.84, and 0.94 are shown in Fig. 1. The pressures along top and bottom generators (shown typically for $M_\infty=0.84$) are in good agreement and confirm zero in-

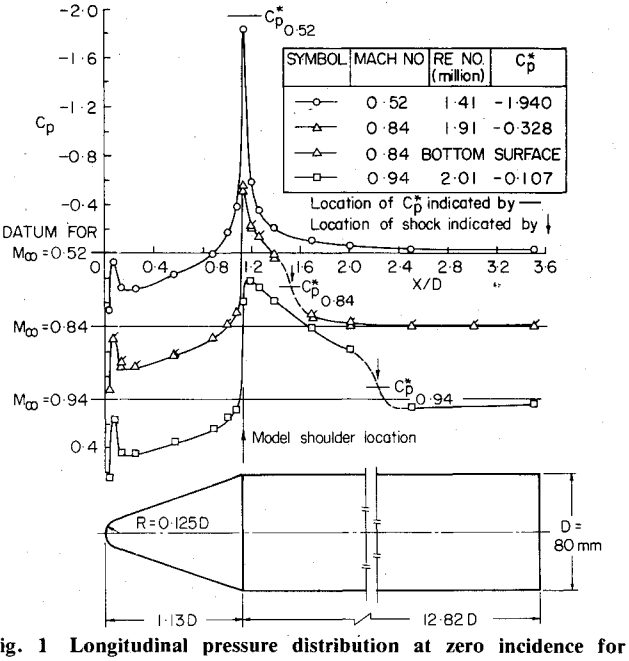

Fig. 1 Longitudinal pressure distribution at zero incidence for $M_\infty=0.52$, 0.84, and 0.94.

Received Sept. 25, 1977; revision received Nov. 28, 1977.

Index category: Transonic Flow.

*Head, Aerodynamics Division.
†Scientist, Aerodynamics Division.

cidence. The values of $C_p{}^*$ (pressure coefficient corresponding to local sonic conditions) are also shown in these plots. Since the flow around the nose-cone junction is locally subsonic, the discontinuity in longitudinal surface curvature gives rise to a local overexpansion in the pressure distribution. The strong adverse pressure gradient suggests the possibility of a small separation bubble and, as will be seen later, this was confirmed by the oil flow pattern. However, since this negative peak is obtained from a single pressure point around the region, the precise magnitude is somewhat uncertain.

The flow is subsonic everywhere for $M_\infty = 0.52$. At Mach numbers 0.84 and 0.94, the flow expands to supersonic speed at the shoulder almost abruptly. The expansion waves from the shoulder reflect back from the sonic boundary as compression waves and result in a gradual deceleration of the supersonic flow downstream of the shoulder. However, at some distance downstream of the shoulder, these compression waves coalesce and result in a shock. Downstream of the shock, the static pressure gradually reverts to nearly freestream value. From the pressure plots, it is apparent that the supersonic region increases with increasing Mach number, and consequently, the terminal shock moves downstream with increase in Mach number.

It is interesting to compare the results obtained in the present investigations with those presented in Refs. 1 and 3, at least qualitatively. It is confirmed that for $M_\infty < 1$, the supersonic region increases with increasing Mach number, and the terminal shock moves downstream. However, the strength of the terminal shock initially increases with Mach number and later decreases. At $M_\infty \simeq 1$, there is virtually no shock. The maximum shock strength occurs at approximately $M_\infty = 0.8$-0.85. It is further noticed that, in the range $M_\infty = 0.9$-0.95, the static pressure after the shock is higher than the freestream static pressure before it gradually reverts back to the freestream value far downstream.

These trends can be explained from the following physical considerations. As M_∞ increases beyond the value at which the sonic velocity is just reached at the shoulder, the supersonic Mach number downstream of the shoulder initially increases and results in an increased shock strength. However, at some M_∞ less than 1, the supersonic Mach number just downstream of the shoulder corresponds to the maximum attainable due to the complete turning of the sonic flow over the corner. With further increase of M_∞ and corresponding increase of the supersonic region, the effect of recompression due to reflected waves from the sonic line could only result in a reduced supersonic Mach number on the surface at the termination of the supersonic region. At M_∞ close to sonic value, when the supersonic region extends almost all the way up to downstream infinity from the shoulder, one can expect a smooth deceleration downstream of the shoulder without any shock.

The reason for the static pressure on the cylinder just downstream of the shock at some Mach numbers (at $M_\infty = 0.94$ in the present investigation) being higher than the freestream value is not quite obvious. However, one plausible explanation that occurs to the authors is that the flow may acquire sufficient concave curvature due to deceleration of supersonic flow over the cylinder and/or the shock-wave/boundary-layer interaction to permit pressures on the surface to be slightly higher than the freestream value.

Longitudinal Pressure Distributions at Incidence

Figures 2 and 3 show the longitudinal pressure distributions on both leeward and windward sides of the model for nominal angles of attack of 0, 5, and 10 deg at $M_\infty = 0.52$ and 0.94.

At $M_\infty = 0.52$, the overall surface pressure characteristics remain qualitatively similar for different angles of attack. As the angle of attack is increased, the overexpansion at the nose-cone junction becomes less pronounced on the windward side and more pronounced on the leeward side. This results from

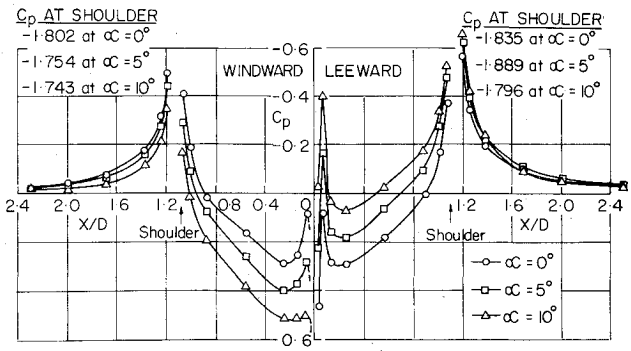

Fig. 2 Longitudinal pressure distribution at incidence for $M_\infty = 0.52$.

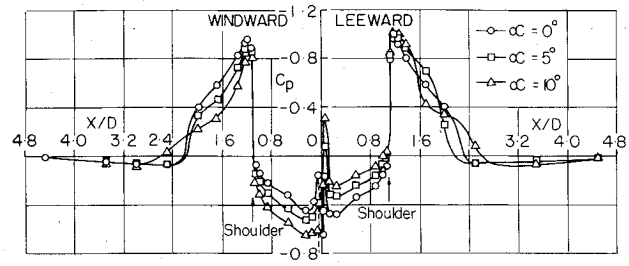

Fig. 3 Longitudinal pressure distribution at incidence for $M_\infty = 0.94$.

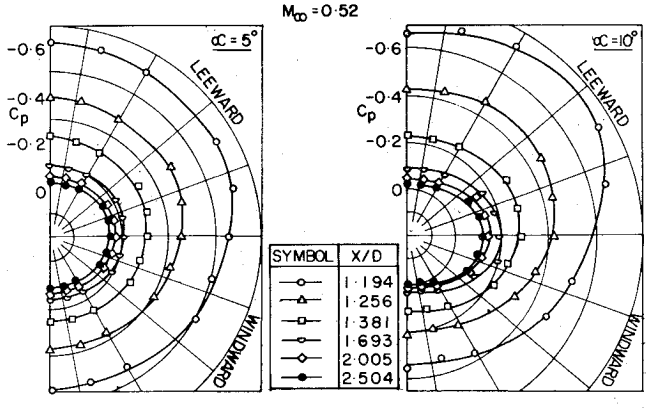

Fig. 4 Circumferential pressure distribution for $M_\infty = 0.52$ at $\alpha = 5$ and 10 deg.

the movement of the stagnation point toward the junction on the windward meridian. Even beyond the shoulder, the pressure on the windward side increases with α, whereas on the leeward side it decreases, although the effect is less pronounced particularly on the leeward side.

At $M_\infty = 0.94$, upstream of the cone-cylinder shoulder, the pressure increases on the windward side and decreases on the leeward side, as incidence is increased, just as at $M_\infty = 0.52$. However, at the shoulder, the variation in C_p with incidence is negligible. At a 5-deg incidence, the terminal shock moves slightly downstream on the windward side and slightly upstream on the leeward side. A similar observation is made in Ref. 1. However, at a 10-deg incidence, the pressure distribution suggests a γ shock on the leeward side, and hardly any shock on the windward side.

Circumferential Pressure Distribution at Incidence

Figures 4 and 5 show the circumferential pressure distributions at $M_\infty = 0.52$ and $M_\infty = 0.94$ at angles of incidence of 5 and 10 deg for a few representative longitudinal stations downstream of the shoulder. At $M_\infty = 0.52$, when the flow on the model is everywhere subsonic, the circumferential

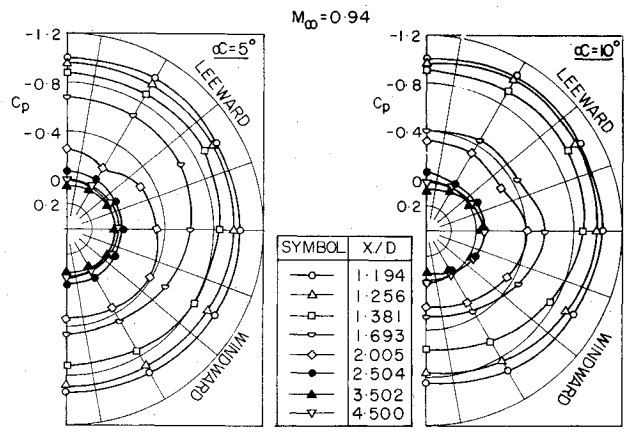

Fig. 5 Circumferential pressure distribution for $M_\infty = 0.94$ at $\alpha = 5$ and 10 deg.

pressure distributions are smooth. The minimum C_p occurs at the leeward generator for stations near the shoulder where the effect of the stagnation point movement on the nose predominates. On the other hand, far downstream from the shoulder, the circumferential C_p variation is mainly due to cross flow. At $M_\infty = 0.94$, at stations upstream of the shock, the circumferential pressure distribution is smooth for both $\alpha = 5$ and 10 deg. At $\alpha = 5$ deg, waviness in the circumferential pressure distributions is observed for $X/D = 2.005$, which is close to the shock location on the leeward side (Fig. 3).

At $\alpha = 10$ deg, a shock first appears on the leeward side around $X/D = 1.6$ resulting in the waviness in the circumferential pressure distribution for $X/D = 1.693$. The occurrence of waviness in the pressure distribution may be attributed to nonaxisymmetric shock formation.

Flow Visualization at Zero Incidence

Figure 6 presents photographs of the surface flow patterns taken at $M_\infty = 0.52$, 0.75, 0.8, 0.85, 0.9, and 0.925 at zero incidence and also sketches interpreting these flow patterns. At the nose-cone junction, accumulation of oil followed by a relatively oil-free region seen at all Mach numbers is indicative of local separation. A close look at the oil pattern near the shoulder at $M_\infty = 0.52$ indicates a separation bubble of very short length; such a bubble is distinctly indicated at $M_\infty = 0.75$ (Fig. 6a).

At $M_\infty = 0.8$ (Fig. 6b) there is no oil accumulation at the shoulder, whereas an accumulation appears downstream. This is interpreted as separation caused by the terminal shock of the local supersonic flow. A similar pattern has been reported by Ericsson.[2] The removal of the suspension at the reattachment region following separation is also clearly visible.

From the side view, it is seen that the flow is not axisymmetric. The observed pattern is thought to be the result of the vorticity in the bubble being shed at the sides as shown in the accompanying sketch. A similar phenomenon is also observed at $M_\infty = 0.85$. This phenomenon appears to confirm the conclusion of the earlier work[5] that axisymmetric flow is hard to attain in practice, particularly under separated flow conditions. Since the flow pattern remained the same with reference to the tunnel configuration even when the model was rotated, it is believed that the asymmetric wall configuration (top/bottom being different from sides) could be triggering the shedding of the vortex from the sides. Although vortex shedding from the sides appears to be predominant, the possibility of there being, in addition, a number of streamwise vortices generated due to the inherent instability[6-8] of concave boundary-layer flow (caused by shock-wave/boundary-layer interaction) cannot be ruled out.

At $M_\infty = 0.9$ (Fig. 6c), the diffused accumulation of oil is perhaps indicative of a reduction of the skin friction locally at the shock without boundary-layer separation, since no reattachment line is visible. At $M_\infty = 0.925$ the oil is even more diffused, resulting from decreasing shock strength with Mach number approaching unity.

The approximate shock locations obtained from the oil visualization studies up to $M_\infty = 0.925$ were checked with the

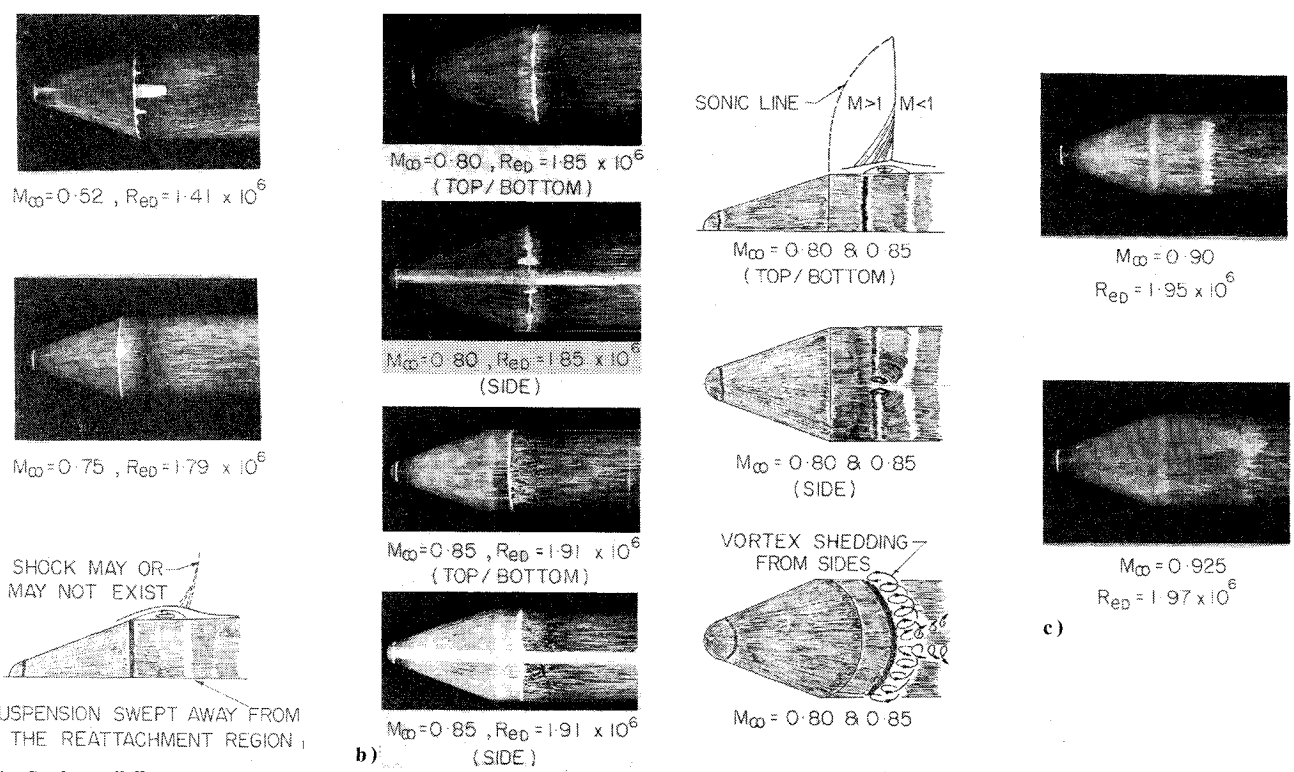

Fig. 6 Surface oil flow patterns at zero incidence for various Mach numbers: a) flow with separation at the shoulder; b) flow with shock-induced separation, reattachment, and vortex shedding from side; c) flow with shock but no separation.

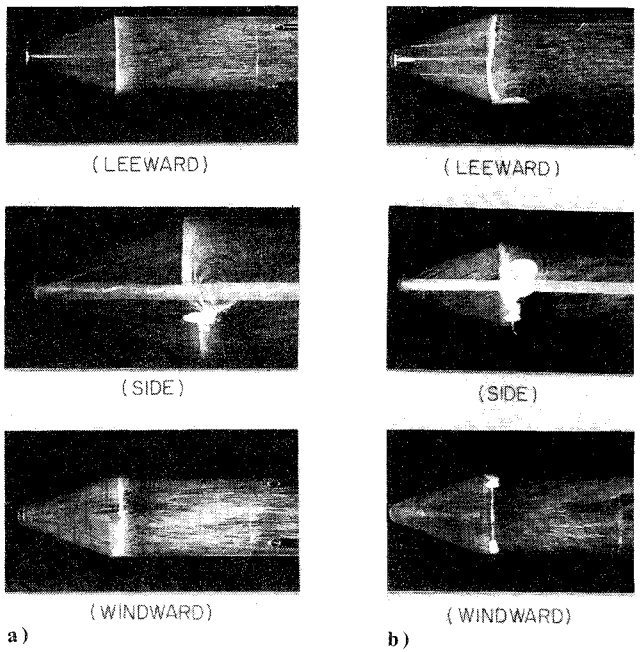

Fig. 7 Surface oil flow pattern at incidence: a) $M_\infty = 0.8$, $\alpha = 5$ deg, $Re_D = 1.85 \times 10^6$; b) $M_\infty = 0.8$, $\alpha = 10$ deg, $Re_D = 1.1. \times 10^6$; c) interpretation of surface flow pattern.

approximate shock locations deduced from pressure measurements, and good agreement was found. The shock moves downstream with Mach number, gradually at first and very rapidly as $M_\infty = 1.0$ is approached. The shock strength initially increases with M_∞ and later weakens as M_∞ approaches 1.0.

Flow Visualization at Incidence

Figure 7 presents photographs of the flow patterns obtained at $M_\infty = 0.8$ for angles of incidence of 5 and 10 deg. The leeward and side views suggest that leeward separation has moved to the shoulder, whereas on the windward side the flow pattern continues to be similar to that at zero incidence. The vorticity in the windward shock-induced separation bubble is shed from the sides in the form of strong vortices, which is clearly visible in the side view. The inferred flow pattern is sketched in Fig. 7c.

Conclusions

The following conclusions can be drawn from the pressure measurements and flow pattern data:

1) Discontinuity of longitudinal curvature at the nose-cone junction results in local separation.

2) At zero incidence, the terminating shock on the cylindrical portion moves downstream slowly at first, and increases in strength with increasing Mach number. Later it moves very rapidly and weakens as the freestream Mach number approaches unity.

3) At incidence, the nonaxisymmetric terminal shock on the cylindrical portion gives rise to waviness in the circumferential pressure distribution. The vorticity in the windward shock-induced separation bubble is shed from the sides in the form of strong vortices.

4) As indicated by earlier work, axisymmetric flow is hard to attain in practice, particularly under separated conditions. This is confirmed in the present studies from flow patterns at $M_\infty = 0.8$ and 0.85 at zero incidence.

Acknowledgment

The authors acknowledge the service rendered by the National Aeronautical Laboratory 4-ft tunnel staff in carrying out these tests and reducing the data.

References

[1] Ericsson, L. E., "Steady and Unsteady Terminal-Shock Aerodynamics on Cone-Cylinder Bodies," NASA CR-61560, Oct. 1967.

[2] Ericsson, L. E., Reding, J. P., and Guenther, R. A., "Analytic Difficulties in Predicting Dynamic Effects of Separated Flow," AIAA Paper 70-762, 1970.

[3] Tsuying Hsieh, "Flow Field Study About a Hemispherical Cylinder in Transonic and Low Supersonic Mach Number Range," AIAA Paper 75-83, Jan. 1975.

[4] *Users Manual—4-Ft Trisonic Wind Tunnel,* National Aeronautical Laboratory, Bangalore, India, Jan. 1973.

[5] Reding, J. P., Guenther, R. A., Ericsson, L. E., and Leff, A. D., "Nonexistence of Axisymmetric Separated Flow," *AIAA Journal,* Vol. 7, July 1969, pp. 1374-1375.

[6] Ginoux, J. J., "The Existence of Three-Dimensional Perturbations in the Reattachment of a Two-Dimensional Supersonic Boundary Layer After Separation," AGARD Report 272, April 1960.

[7] Roshko, A. and Thomke, G. J., "Observations of Turbulent Reattachment Behind an Axisymmetric Downstream-Facing Step in Supersonic Flow," *AIAA Journal,* Vol. 4, June 1966, pp. 975-986.

[8] Hopkins, E. J., Keating, S. J., and Bandettini, A., "Photographic Evidence of Streamwise Arrays of Vortices in Boundary Layer Flow," NASA TN D-328, 1960.